Current Applied Physics 25 (2021) 55–61

Contents lists available at ScienceDirect

Current Applied Physics

journal homepage: www.elsevier.com/locate/cap

Mössbauer and MCD spectroscopy of the Fe_3S_4 nanoparticles synthesized by the thermal decomposition method with two different surfactants

Ruslan D. Ivantsov [a,*], Chun-Rong Lin [b,**], Oxana S. Ivanova [a,c], Roman R. Altunin [c], Yuriy V. Knyazev [a,c], Maxim S. Molokeev [a,c], Sergey M. Zharkov [a,c], Ying-Zhen Chen [b], En-Szu Lin [b], Bing-Yi Chen [b], Nikolai P. Shestakov [a], Irina S. Edelman [a]

[a] Kirensky Institute of Physics, FRC KSC SB RAS, Krasnoyarsk, 660036, Russia
[b] Department of Applied Physics, National Pingtung University, Pingtung City, Pingtung County, 90003, Taiwan
[c] Siberian Federal University, Krasnoyarsk, 660041, Russia

ARTICLE INFO

Keywords:
Greigite
Thermal decomposition
Surfactants
Mössbauer effect
FT-IR spectra
Magnetic circular dichroism

ABSTRACT

Greigite (Fe_3S_4) nanoparticles (NPs) were fabricated by the thermal decomposition method using two different surfactants: oleylamine (OLA) and 1-hexadecylamine (HDA). In both cases, the synthesized NPs were characterized as the Fe_3S_4 nanocrystals with minor inclusions of Fe_9S_{11} phase. FT-IR spectroscopy and thermogravimetric analysis allow concluding about OLA or HDA shells covering magnetic core of NPs. Mössbauer spectra has revealed deviations of iron ions distribution among crystal positions from that presented in literature for pure greigite. In accordance with these deviations, the pronounce changes are observed in the magnetic circular dichroism (MCD) spectra which manifest themselves as the spectrum shift to higher energies of electromagnetic waves and redistribution of the MCD maximum intensities. These effects are associated with a change in the density of electronic states in the samples due to the redistribution of iron ions between octahedral and tetrahedral positions in nanocrystals under the influence of surfactants.

1. Introduction

Modern techniques and technologies cannot be imagined without the use of nanostructured magnetic materials. Until recently, nanostructures and ensembles of nanoparticles (NPs) of the transition metal oxides, mainly iron, were considered. Currently, there is an increasing interest in chalcogenides, that is, compounds of transition metals with sulfur, selenium, and tellurium. The transition from the ionic character of bonds in oxides to the covalent character in chalcogenides leads to the appearance of transport and optical properties, similar to those of semiconductors or even metals, and the emergence of new fields of application. One of the promising groups of such materials is the family of iron sulfides $Fe_{1-x}S$, in particular, greigite, Fe_3S_4 ($x = 0.25$), which is a ferrimagnet with an inverted spinel structure, isostructural to magnetite Fe_3O_4, that is it refers to the Fd-3m space group. The S^{2-} ions form a cubic face-centered lattice with the tetrahedral and octahedral interstices. Tetrahedral sites (A-sites) are occupied by Fe^{3+} ions only while octahedral ones are populated by ½ of Fe^{3+} ions and Fe^{2+} ions equally. Iron ion magnetic moments in octahedral and tetrahedral sites are ordered antiferromagnetically and give the resulting magnetic moment of 59 Am^2kG^{-1} (3.13 μ_B/f.u.) at room temperature [1]. Particular attention is paid to the greigite NPs [2,3] in connection with the prospects of using their unique properties in a wide variety of fields, ranging from already developed adsorbents and catalysts [4,5], anodes for lithium batteries [6,7], sensors [8], and medical applications [9] up to the prediction of strong permanent magnets that do not contain rare earth elements [10] and devices for absorbing electromagnetic radiation [11]. It should be noted that in real technological experiments, along with greigite, other phases similar in composition, such as pyrrhotite, Fe_7S_8 [12] and, smythite, Fe_9S_{11} [13] can also appear. Thus, the synthesis of single-phase sulfide nanoparticles $Fe_{1-x}S$ is not an easy task. Another serious problem concerns the prevention of NPs agglomeration due to magnetic interactions and high values of surface energy, as well as the NPs oxidation by atmospheric oxygen. This problem is usually solved by using organic surfactants. For the iron oxides NPs, numerous studies of the effect of surfactants of various nature on the properties of

* Corresponding author.
** Corresponding author.
E-mail addresses: ird@iph.krasn.ru (R.D. Ivantsov), crlinspin@gmail.com (C.-R. Lin).

https://doi.org/10.1016/j.cap.2021.02.013
Received 13 September 2020; Received in revised form 6 February 2021; Accepted 21 February 2021
Available online 8 March 2021

Table 1
The expected NPs phase compositions, the brief description of the synthesis process, and phase composition according to the results of the investigation.

Sample name	Expected composition	Description	Phase composition according to XRD and Mössbauer* data
FS-OLA	Spinel Fe_3S_4	S-powder+Fe $(NO_3)_3{\cdot}9H_2O$+**OLA**+OA (240 °C, 30min.)	Fe_3S_4 *Admixture ~2% Fe_9S_{11}
FS-HDA	Spinel Fe_3S_4	S-powder+Fe $(NO_3)_3{\cdot}9H_2O$+**HDA**+OA (240 °C, 30min.)	Fe_3S_4 *Admixture ~5% Fe_9S_{11}

synthesized NPs have been carried out (for example, [14–16]). In Ref. [14] oleic acid (OA), sodium dodecylsulfate (SDS), polyvinyl alcohol (PVA), and olive oil were studied, and each of these surfactants influenced the properties and magnetic phase composition of oxide NPs. For example, in the case of SDS, the maghemite phase, γ-Fe_2O_3, was detected in the samples along with the main phase Fe_3O_4. Contrary to situation with oxide NPs, only a few works we have managed to find in current literature concerning the use of surfactants in the process of the $Fe_{1-x}S$ NPs synthesis [17]. A present paper is devoted to the synthesis of the Fe_3S_4 NPs by the thermal decomposition method using two different surfactants and to a study of their structure and magnetic properties in comparison with properties of pure greigite NPs investigated earlier by several co-authors of the present paper [18]. The NPs crystal structure and morphology were studied with the X-ray diffraction and transmission electron microscopy, their phase composition was determined with the Mössbauer spectroscopy, and magnetic properties of the samples were studied using one of the most informative magneto-optical effects - magnetic circular dichroism (MCD) in transmitted light. Since MCD is a linear function of magnetization, its field and temperature dependences reflect similar dependences of the magnetization of the samples. On the other hand, MCD is due to the electron transitions between the ground and excited energy levels or bands in a substance, and therefore the study of the MCD spectral dependences makes it possible to obtain information on the change in the energy structure of a material depending on the synthesis conditions.

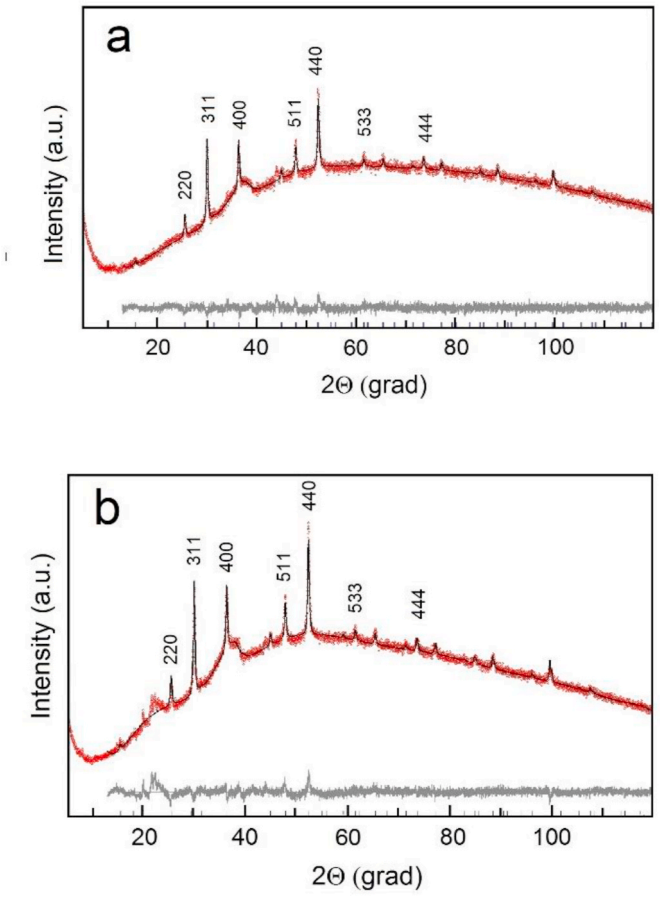

Fig. 1. Rietveld refined XRD patterns (red lines– XRD data, black – theoretical fits to the XRD data) and the difference pattern between the observed data and the theoretical fit (at the bottom) for samples OLA (a) and HDA (b). The peaks of greigite are indicated. The broad background signals can be associated with the presence of organic components in the samples as it will be seen from the FT-IR spectra. (For interpretation of the references to colour in this figure legend, the reader is referred to the Web version of this article.)

2. Experimental section

2.1. Synthesis of nanoparticles

Iron sulfide NPs were synthesized through thermal decomposition of the mixture of complexes of the fatty amines: oleylamine, $C_{18}H_{35}NH_2$, – sample OLA, and 1-hexadecylamine, $C_{16}H_{35}N$, – sample HDA, with iron nitrate, ($Fe(NO_3)_3{\cdot}9H_2O$), sulfur powder, and oleic acid (OA). OLA and HDA being kinds of alkyl-amines were chosen here as surfactants because alkyl-amines were shown to be quite suitable to synthesize metal sulfide nanocrystals [19]. Oleic acid was added to provide more rapid kinetics. The typical conditions were as follows. In the first case, 1 g of iron nitrate ($Fe(NO_3)_3{\cdot}9H_2O$), 0.1587 g of sulfur powder, 10 ml of oleylamine (OLA), and 5 ml of oleic acid (OA) were put into a three-neck flask equipped with an inlet of argon gas, condenser, magnetic stirrer, thermocouple, and heating mantle. After the argon gas was introduced into the system for 10 min, the mixture was heated to 120 °C and maintained at this temperature for 0.5 h, and then the temperature was rose to 200 °C aged for 0.5 h. Finally, the reaction mixture was heated up to 240 °C and aged for 0.5 h. In the second case, 10 g of HDA was used instead of OLA. Otherwise, the process went along the same route as described above. After the mixture cooled down to room temperature, the obtained NPs can be separated from the suspension with a magnetic field. To remove the excess organic solvent and by-products completely, the products were washed several times with hexane by the magnetic decantation. The reaction parameters used in the synthesis of a series of iron sulfide NPs are listed in Table 1.

2.2. Measurement methods

The powder diffraction data for Rietveld analysis were collected at room temperature with a Bruker D8 ADVANCE powder diffractometer (Cu-Kα radiation) and linear VANTEC detector. The step size of 2θ was 0.016°, and the counting time was 5 s per step. Rietveld refinement was performed by using TOPAS 4.2 [20].

Morphology of the synthesized NPs was examined using a JEM-2100 transmission electron microscope (JEOL Ltd.) operating at an accelerating voltage of 200 kV. The microscope was equipped with an energy dispersive spectrometer (EDS), Oxford Instruments, what was used to control the elemental composition of the samples. Selected-area electron diffraction (SAED) was used to determine the structure of separate NPs.

Fourier transform infrared absorption (FT-IR) spectra were recorded with the VERTEX 70 (Bruker Optik GMBH) spectrometer in the spectral region of 400 ÷ 4000 cm^{-1} with spectral resolution 4 cm^{-1}. To obtain the spectra, tablet samples were prepared containing OLA or HDA NPs. The round tablets were of about 0.5 mm thick and of 13 mm in diameter and had a weight of 0.140 g. The tablet were prepared as follows: in less than 0.001 g of nano-powders were thoroughly ground with 0.14 g of KBr and were subjected to the cold pressing at 10000 kg. The FT-IR spectrometer was equipped a Globar as a light source and a wide band KBr beam splitter and RT-DLaTG as a detector (Bruker Optik GMBH).

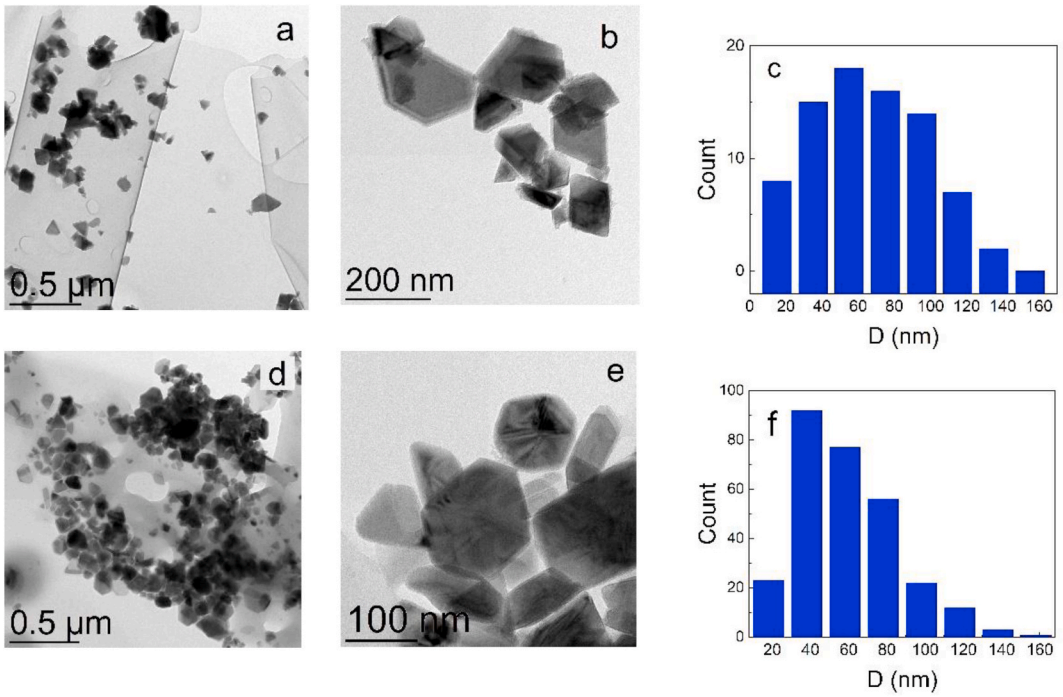

Fig. 2. TEM images in different scales of the FS-OLA (a, b) and FS-HDA (d, e) NPs, and histograms of the NPs size distribution for these two samples (c and f), correspondingly.

The differential Scanning Calorimeter DSC 204 F-1 Phoenix (NETZSCH) was used to estimate the strength of the surfactants bonding with the magnetic core.

The Mössbauer effect spectra of the samples were obtained on an MS-1104Em spectrometer in transmission geometry with a ^{57}Co (Rh) radiation source at 300 K. The processing was carried out in two stages. At the first stage, possible nonequivalent positions of iron in the sample were determined by calculating the probability distributions of magnetic hyperfine fields. In accordance with the results obtained, a preliminary spectrum model was formed. At the second stage, the model spectrum was fitted to the experimental one by varying the entire set of hyperfine parameters using the linear approximation of the least squares' method.

Magnetic properties of the samples were studied using MCD in transmitted light, as it was mentioned in the Introduction. For the measurements, transparent composite plates containing NPs were prepared: the NPs powder was mixed with a transparent dielectric silicone-based adhesive ("Rayher" art. Nr. 3338100 80 ml) in a weight ratio of 0.5/100, and measures were taken to obtain their uniform distribution in the matrix. The mixture was placed between two thin glass plates lined with wires 0.15 mm in diameter and solidified. The low concentration of magnetic powder allowed us to eliminate interactions between NPs. The MCD was measured according method used in Ref. [21] in normal geometry: directions of the magnetic field and of the circularly polarized light wave propagation were normal to the plane of the plates. Modulation of the light wave polarization from right to left circular relative to the direction of the magnetic field was used to increase the sensitivity of measurements. MCD was measured as the difference between the optical densities of the sample ($\Delta D = D_+ - D_-$ for right (+) and left (-) polarized waves in the spectral range 1.25–3.5 eV in a magnetic field of 1.3 T at a temperature of 300 K and in a field of 0.3 T at lower temperatures. The measurement accuracy was about 10^{-4}, and the spectral resolution was 20–50 cm^{-1}, depending on the wavelength.

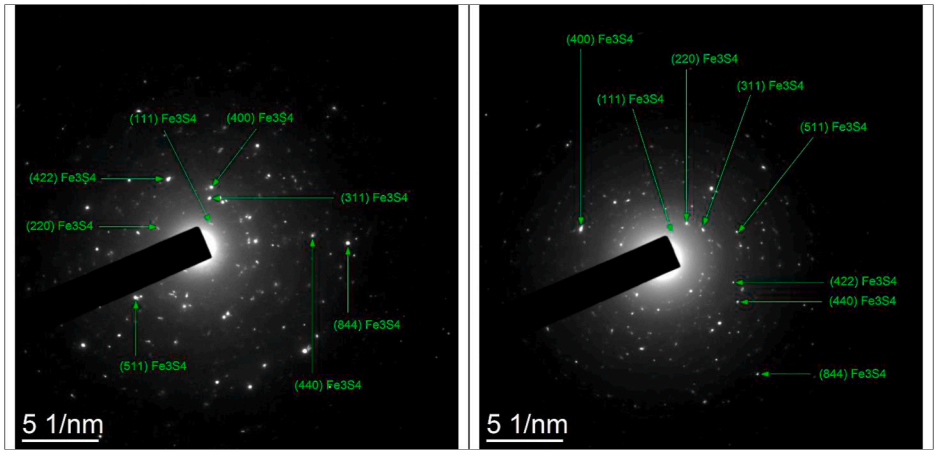

Fig. 3. SAED patterns for NPs in the OLA (left panel) and HDA (right panel) samples. Green arrows mark the main Fe_3S_4 phase reflexes. (For interpretation of the references to colour in this figure legend, the reader is referred to the Web version of this article.)

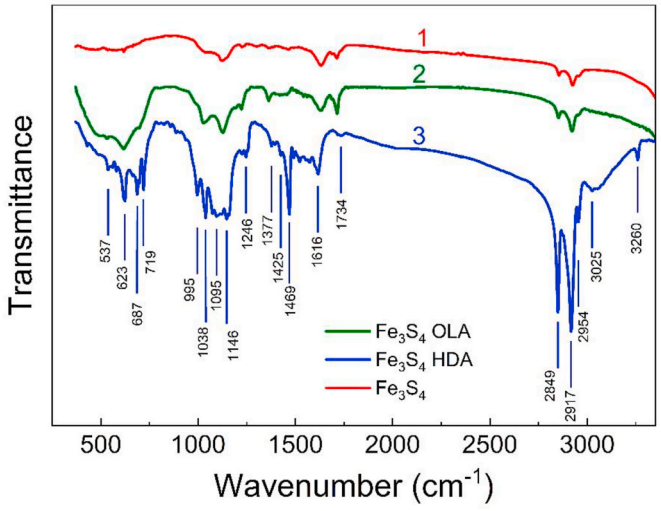

Fig. 4. FT-IR transmission spectra of the Fe_3S_4 nanoparticles (1) synthesized with the polyol mediated process [18], OLA (2) and HDA (3) samples.

3. Results and discussion

The difference Rietveld plots for both powdered samples are presented in Fig. 1. The series of the peaks in the XRD patterns for these samples are characteristic for the cubic Fe_3S_4 structure (PDF card No. 16–0713). No distinct peaks belonging to other iron sulphides or oxides are observed in the patterns although the difference curves show weak disturbances in the range of angles 2θ = 20–50 deg. In this angles interval, the series of weak reflections of smythite, Fe_9S_{11}, and pyrrhotite, Fe_7S_8, were observed in Ref. [22]. Besides the (311) reflex of greigite coincides, practically, with the (101) reflex of smythite and the (200) reflex of pyrrhotite. However, judging by the intensity of disturbances, the proportion of such phases does not exceed 5%. The refines lattice parameter and cell volume of Fe_3S_4 nanocrystals were a = 9.8791(9) Å and V = 964.2(3) $Å^3$ for the OLA sample, and a = 9.8772(8) Å and V = 963.6(2) $Å^3$ for the HDA sample in an agreement with the literature data 9.8719(1) Å in Ref. [2].

For both samples, the electron microscope observation revealed NPs of different shapes and with a large size dispersion. Examples are shown in Fig. 2 for fragments of the FS-OLA (a, b) and FS-HDA (d, e) samples in different scales. Regular hexagons and parts of hexagons are seen in photos. Some changes in the density of the NPs image can be seen at their edges, which may be due to the presence of an organic shell. It is also seen that there is no contact between closely spaced NPs, a gap remains between them, which may be due to the presence of an organic coatings. As seen in histograms (Fig. 2 d and f), the NPs size distribution is narrower for the FS-HDA sample, and the distribution maximum corresponds to smaller NPs size in this case.

SAED patterns (Fig. 3) confirmed the NPs good crystallinity, and the crystal structure belonging to the Fe_3S_4 of Fd-3m space group. The low admixture of sulfur compounds with the higher S content could not be excluded. Negligible amount of sulfur has been noticed in the HDA sample. According to EDS data, the Fe and S atomic concentrations were Fe - 42 at. %; S - 58 at. % and Fe - 40 at. %, S - 60 at. % for OLA and HDA samples, respectively, that is the sulfur concentration in the samples was a little bit higher comparing to Fe_3S_4: Fe 42.8 at. % S 57.2 at. %. It can be associated with the presence of the free sulfur or the small amount of the other sulphides phases with higher Fe concentration such as Fe_7S_8 or Fe_9S_{11}.

The FT-IR transmission spectra of OLA and HDA samples are shown in Fig. 4 in comparison with the spectrum of the Fe_3S_4 NPs synthesized earlier with the polyol mediated process [18]. In the last case, several very weak lines in the regions of 996–1469, 1620–1730, and near 3000

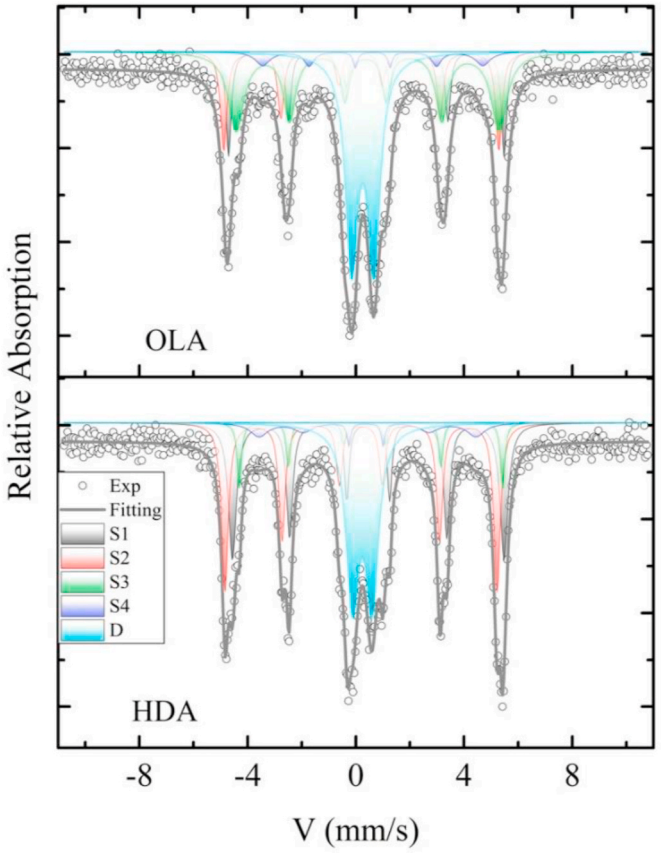

Fig. 5. Mössbauer spectra of two samples at room temperature.

cm^{-1} are observed in the spectrum (curve 1) which does not change absolutely at the sample heating up to 850 °C. The sample mass does not change also. Thus, it can be argued that these NPs are chemically stable and the observed lines can be ascribed to S–S stretching bonds, and S–O and H–O bonds arising because of the samples moisturizing in atmosphere, similar to the interpretation of the FT-IR spectrum of FeS_2 NPs presented in Ref. [23].

In the OLA sample spectrum (curve 2) new feature appears in the region of 400–720 cm^{-1} and the feature at 996-1469 cm^{-1} becomes more intense and better resolved. As concerns the first of these groups, the observed peaks can be ascribed to Fe–O, or C–S bending modes, or to the out of plane N–H bending mode. The sample is resistant to heat in the argon atmosphere up to 300 °C. The content of the modifier in the sample is about 11% according to the weight loss at heating to 850 °C. After such heating, the spectrum is converted to the first sample spectrum (curve 1).

The HDA sample spectrum (curve 3) contains the same set of peaks as the OLA sample but rather intense and better resolved. Since the samples differ from each other only in the nature of the amines, we can confidently assert that the peaks observed in the HDA sample spectra are due to the presence of hexadecylamine. Indeed, the set of two intense peaks at 2849 and 2917 $cm^{-1}$and much weaker peaks at 2954 and 3260 cm^{-1} as well peaks at 1469 and 1617 cm^{-1} are very close to that observed for hexadecylamine and silver and gold NPs capped with hexadecylamine in Ref. [24]. At that, the most prominent peaks at 2917 and 2849 cm^{-1} can be ascribed to C–H stretching of terminal CH_3 and CH_2 group of alkyl chain of HDA, according to Ref. [23]. Note, that oleic acid was used in the synthesis of OLA and HDA samples in the same amount. So, one can expect its contribution in the spectrum as low intense peaks at ~2928 and ~2858 cm^{-1} corresponding to the asymmetric and symmetric stretching vibrations of CH_2 group, respectively [25]. They seem to be indistinguishable in the background of the above mentioned intense

Table 2
Mössbauer parameters of the samples. IS is the chemical isomer shift relative to α-Fe, H_{hf} is the hyperfine field at iron nuclei, QS is the quadrupole splitting, W is the width of the Mössbauer line at half maximum, dH is the degree of inhomogeneity of the hyperfine field at iron nuclei, A is the relative population of the position.

	IS, mm/s ±0.005	H_{hf}, T, ±0.3	QS, mm/s ±0.01	W, mm/s ±0.01	dH mm/s ±0.01	A % ±1.0	Positions Description
OLA							
S1	0.294	31.6	0.05	0.27	0	17	Fe_3S_4 –A
S2	0.527	31.6	−0.13	0.23	0	14	Fe_3S_4 –B
S3	0.506	30.2	0.14	0.32	0.38	33	Fe_3S_4 –B
S4	0. 562	25.3	0	0.31	0.197	3	Fe_9S_{11}
D	0.368	–	0.81	0.55	–	34	Fe_3S_4-SPM
HDA							
S1	0.298	31..2	0.00	0.24	0.00	30	Fe_3S_4 –A
S2	0.570	312	0	0.18	0.18	29	Fe_3S_4 –B
S3	0.547	30.2	0.49	0.18	0	7	Fe_3S_4 –B
S4	0.527	25.5	0.04	0.55	0	5	Fe_9S_{11}
D	0.344	–	0.73	0.56	–	29	Fe_3S_4-SPM

peaks of hexadecylamine. The HDA sample is thermally stable at heating up to 180 °C. Heating to 850 °C in the argon atmosphere leads to the weight loss of 56% and the spectrum conversion to curve 1. Judging by the weight loss upon heating, the organic coating of the magnetic core is much thicker in the HDA sample as compared to the OLA sample, which agrees with the electron-microscope image in Fig. 2 e.

Mössbauer spectra for both samples are shown in Fig. 5. The processing results are collected in Table 2. The best fittings of the modelled spectrum to the experimental ones were obtained taking into account several sextets and one doublet. As mentioned in the introduction, Fe_3S_4 has a spinel crystal structure, which is characterized by the presence of Fe^{3+} cations in tetrahedral and octahedral and Fe^{2+} cations in octahedral positions. The different local environment of iron in these positions leads to differences in their Mössbauer parameters, first of all, the isomeric chemical shift (IS), which depends on the electron density on the nucleus. As shown in Refs. [1,18,26,27] the characteristic IS for tetrahedral coordinated iron in Fe_3S_4 is 0.28–0.43 mm/s. That is why, the S1 sextets in the observed spectra can be ascribed to Fe ions occupying tetrahedral positions (A). Two other sextets S2 and S3 are logical to be referred to the Fe ions in octahedral positions (B1 and B2) in accordance with the significantly greater isomer shift. Such a change in the value of IS, as already mentioned, is due to different six's electron density on the iron nuclei, which is determined by the degree of delocalization of iron electrons at the formation of chemical bonds. Some authors (e. g., Ref. [18]) do not distinguish these positions and consider one sextet with IS shift 0.5–0.55 mm/s to the $Fe^{2.5+}$ ions associating such valence value with the fast electron exchange Fe^{3+} and Fe^{2+} ions in octahedral positions characteristic for Fe_3S_4. However, here we preferred to separate the two positions, since some distribution over the H_{hf}: octahedral (B2) iron cations are characterized by S2 sextet with an increased H_{hf}. This may indicate the appearance of an additional magnetic bonds or cation vacancies for such cations.

Sextet S4 is characterized by significantly lower value of H_{hf} comparing to that observed for Fe_3S_4 but close to H_{hf} obtained in Ref. [28] for one of the sextets in the Mössbauer spectrum of smythite (Fe_9S_{11}). As it seen from Table 2, the portion of this component is very small. And, at last, the rather intense doublets (D) indicate a superparamagnetic state at room temperature of about one third of the nanoparticles both for OLA and HDA. This correlates with the presence of nanoparticles with sizes less than 20 nm in both cases (Fig. 2 c and f). The described comparison of the components of the Mössbauer spectra with certain magnetic states of nanoparticles and positions of iron ions is presented in the right column in Table 2.

Note that the population of the tetrahedral positions of the inverted spinel should be half of that in the octahedral ones, which is not

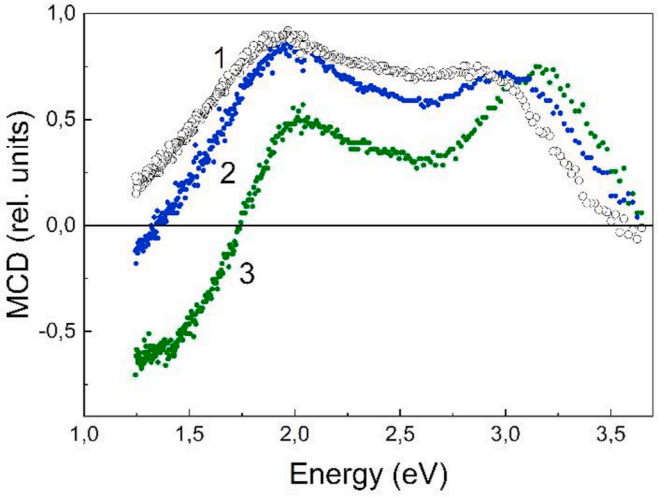

Fig. 6. Room temperature MCD spectra for the Fe_3S_4 NPs, synthesized with the polyol mediated process without surfactants (1), the OLA (2), and HDA (3) samples in magnetic field 5.0 kOe.

observed in the present samples. At that, a deficiency of iron ions in A positions are observed for sample FS-OLA while for FS-HDA sample there are not enough ions in the B positions. At the same time, ration of A and B position populations in the greigite NPs synthesized with polyol mediated process was ~½ analogously to the stoichiometric greigite crystals (Table 1 in Ref. [18]). Assumption is possible that the nature of surfactants has an effect on the distribution of cations over positions occurring in the course of the NPs formation. Different effects of OLA and HDA may be due to the different degree of unsaturation of surfactant molecules. OLA refers to the so-called unsaturated fatty amines [29] while hexadecylamine is saturated amine. As known in chemistry, in saturated hydrocarbons all hydrogen atoms and carbon atoms are bonded together with single bonds, unsaturated hydrocarbons have double or even triple bonds between the carbon atoms. This makes unsaturated hydrocarbons even more reactive than saturated hydrocarbons. Such a difference between chemical activity of two surfactants can play an important role in the NPs formation but this problem requires additional study.

MCD spectra recorded for both samples at room temperature are presented in Fig. 6 together with spectrum of the greigite NPs synthesized earlier with polyol mediated process [30]. All three spectra are close to each other in shape, but the maxima positions change non-monotonically: the energy of maximum near 2 eV stays, practically, unchanged, while higher energy maximum and the point of the MCD curve intersection with the energy axis shift differently to higher energies. The shifts are evidently stronger for the HDA sample, even a new negative peak near 1.3–1.4 eV becomes apparent for this sample. Discussing the origin of the MCD spectrum of greigite NPs, authors of [30] carried out *ab initio* calculations of the bulk Fe_3S_4 band structure by the pseudo-potential method using the plane wave basis within the density functional theory (DFT) in the generalized gradient approximation. They obtained the spin polarized density of states (DOS) for two atomic positions – octahedral and tetrahedral sites of Fe_3S_4. At that, the dominant contribution at the Fermi level resulted from the spin down d-electrons originated from the octahedral iron ions. The MCD spectrum was shown to be formed by the interband excitations from the occupied to empty electronic states with the same spin projections. As can be seen from the characteristics of the spectra of the Mössbauer effect (Table 2), the populations of the octahedral and tetrahedral positions are different for the two types of coatings. This can lead to some changes in the density of states and, consequently, to the observed shift of bands in the MCD spectrum and a redistribution of their intensity.

The MCD dependences on an external magnetic field are shown in

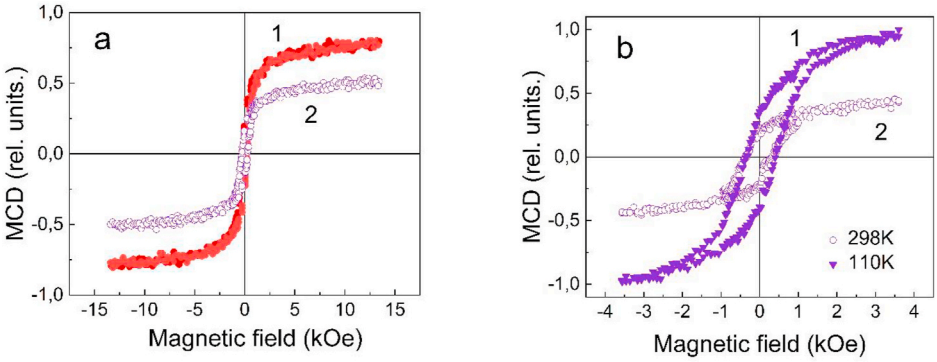

Fig. 7. MCD dependences on magnetic field (a) for OLA (1) and HDA (2) samples at room temperature, and (b) for the HDA sample at two temperatures in lower magnetic field. The dependences are recorded for the wavelength corresponding to the MCD maxima near 2 eV.

Fig. 7. Since the MCD is a linear function of magnetization, its dependence on the magnetic field and temperature reflects similar dependences of the magnetization of the samples. However, the ratio of the MCD values in different samples may differ from the ratio of the magnetizations. Thus, the shape of the curves of the MCD dependence on the external magnetic field can be used to clarify the processes of magnetization reversal of samples. It is seen from Fig. 7 that the presented curves can be considered as a sum of two types of the magnetization processes – ferromagnetic with hysteresis and remnant magnetization and superparamagnetic. The picture is almost the same for both samples: OLA and HDA. Fig. 7 shows the same value of coercivity of the HDA sample for two temperatures, that is, upon cooling to 110 K, a significant part of the NPs remains in a blocked state. A more detailed study of the behavior of the OLA and HDA NPs in a magnetic field is in progress now.

4. Conclusion

Greigite NPs were synthesized by the thermal decomposition method using two types of surfactants – oleylamine, $C_{18}H_{35}NH_2$, (sample OLA) and 1-hexadecylamine, $C_{18}H_{39}NO_2$, (sample HDA). The surfactants type does not effect in the NPs crystal structure. In both cases, Fe_3S_4 nanocrystals with the cubic inverted spinel structure were obtained. Thermogravimetric analysis and FT-IR spectra recorded before and after the samples heating proved the presence of the organic shells around Fe_3S_4 magnetic core in both cases, however this shell is considerably more massive for the HDA sample. Surfactants affect the Mössbauer spectra, leading to different Fe^{3+} and Fe^{2+} distribution over octahedral and tetrahedral crystal positions in the OLA and HDA samples, an appearance of cation vacancies, and the energy bands shift relative to the bands in Fe_3S_4 NPs without shell. HDA shell effects markedly in the MCD spectrum: the spectrum shifts to the higher energy and the maxima intensity redistribution is observed in this sample comparing to the OLA sample and initial Fe_3S_4 sample. This effect is associated with a change in the density of electronic states in the HDA sample due to a change in the distribution of iron ions over crystal positions revealed using the Mössbauer effect.

Declaration of competing interest

The authors declare that they have no known competing financial interests or personal relationships that could have appeared to influence the work reported in this paper.

Acknowledgments

The reported study was funded by Joint Research Project of Russian Foundation for Basic Research N° 19-52-52002 and Ministry of Science and Technology, Taiwan MOST N° 108-2923-M-153-001-MY3 and N° 106-2112-M-153-001-MY3, and by Russian Foundation for Basic Research with Government of Krasnoyarsk Territory, Krasnoyarsk Regional Fund of Science, the research project number 19-42-240005: "Features of the electronic structure, magnetic properties and optical excitations in nanocrystals of the multifunctional magnetic chalcogenides Fe_3S_4 and FeSe". The electron microscopy and electron diffraction investigations were conducted in the SFU Joint Scientific Center supported by the State assignment (#FSRZ-2020-0011) of the Ministry of Science and Higher Education of the Russian Federation. The thermal-gravity measurements were carried out with the differential Scanning Calorimeter DSC 204 F-1 Phoenix (NETZSCH) in the Krasnoyarsk Regional Center of Research Equipment of Federal Research Center «Krasnoyarsk Science Center SB RAS».

References

[1] L. Chang, A.P. Roberts, Y. Tang, B.D. Rainford, A.R. Muxworthy, Q. Chen, Fundamental magnetic parameters from pure synthetic greigite (Fe_3S_4), J. Geophys. Res.: Solid Earth 113 (2008) B06104, https://doi.org/10.1029/2007jb005502.

[2] G. Li, B. Zhang, F. Yu, A.A. Novakova, M.S. Krivenkov, T.Y. Kiseleva, L. Chang, J. Rao, A.O. Polyakov, G.R. Blake, R.A. de Groot, T.T.M. Palstra, High purity Fe_3S_4 greigite microcrystals for magnetic and electro-chemical performance, Chem. Mater. 26 (2014) 5821–5829, https://doi.org/10.1021/cm501493m.

[3] J. Moore, E. Nienhuis, M. Ahmadzadeh, J. McCloy, Synthesis of greigite (Fe_3S_4) particles via a hydrothermal method, AIP Adv. 9 (2019), 035012. https://doi/10.1063/1.5079759.

[4] Y. Zhou, Y. Zhao, X. Wu, W. Yin, J. Hou, S. Wang, K. Feng, X. Wang, Adsorption and reduction of hexavalent chromium on magnetic greigite (Fe_3S_4)-CTAB: leading role of Fe(II) and S(-II), RSC Adv. 8 (2018) 31568. https://doi/10.1039/c8ra06534a.

[5] J. Jencarova, A. Luptakova, N. Vitkovska, D. Matysek, P. Jandacka, Magnetic sorbents biomineralization on the basis of iron sulphides, Environ. Technol. 39 (2018) 2916–2925, https://doi.org/10.1080/09593330.2017.136958.

[6] Z. Jiang, X. Gu, L. Wang, L. Huang, First-principles study of intercalation of alkali ions in FeSe for solid-state batteries, Chem. Phys. Lett. 659 (2016) 230–233, https://doi.org/10.1016/j.cplett.2016.07.040.

[7] X. Wang, Z. Yang, C. Wang, L. Ma, C. Zhao, J. Chen, X. Zhang, M. Xue, Auto-generated iron chalcogenide microcapsules ensure high-rate and high-capacity sodium-ion storage, Nanoscale 10 (2018) 800–806, https://doi.org/10.1039/c7nr08255j.

[8] S. Mlowe, N.S.E. Osman, T. Moyo, B. Mwakikunga, N. Revaprasadu, Structural and gas sensing properties of greigite (Fe_3S_4) and pyrrhotite ($Fe_{1-x}S$) nanoparticles, Mater. Chem. Phys. 198 (2017) 167–176, https://doi.org/10.1016/j.matchemphys.2017.06.012.

[9] J. Liu, X. Guo, Z. Zhao, B. Li, J. Qin, Z. Peng, G. He, D.J.L. Brett, R. Wang, X. Lu, Fe_3S_4 nanoparticles for arterial inflammation therapy: integration of magnetic hyperthermia and photothermal treatment, Appl. Mater. Today 18 (2020) 13, https://doi.org/10.1016/j.apmt.2019.100457, 100457-100457.

[10] X. Zhao, C.Z. Wang, M. Kim, K.M. Ho, Fe-cluster compounds of chalcogenides: candidates for rare-earth-free permanent magnet and magnetic nodal-line topological material, Inorg. Chem. 56 (23) (2017) 14577–14583, https://doi.org/10.1021/acs.inorgchem.7b02318.

[11] J. Luo, Y. Hu, L. Xiao, G. Zhang, H. Guo, G. Hao, W. Jiang, Synthesis of 3D flower-like Fe_3S_4 microspheres and quasi-sphere Fe_3S_4-RGO hybrid-architectures with enhanced electromagnetic wave absorption, Nanotechnology 31 (2020), https://doi.org/10.1088/1361-6528/ab53c4, 085708-085720.

[12] T.J. Bastow, A.J. Hill, ^{57}Fe NMR characterization of pyrrhotite, J. Magn. Magn Mater. 447 (2018) 58–60, https://doi.org/10.1016/j.jmmm.2017.09.047.

[13] Y. Furukawa, H.L. Barnes, Reactions forming smythite, Fe_9S_{11}, Geochem. Cosmochim. Acta 60 (1996) 3581–3591.
[14] P. Arévalo, J. Isasi, A.C. Caballero, J.F. Marco, F. Martín-Hernández, Magnetic and structural studies of Fe_3O_4 nanoparticles synthesized via co-precipitation and dispersed in different surfactants, Ceram. Int. 43 (2017) 10333–10340, https://doi.org/10.1016/j.ceramint.2017.05.064.
[15] R. Harris, P.M. Shumbula, H. van der Walt, Analysis of the interaction of surfactants oleic acid and oleylamine with iron oxide nanoparticles through molecular mechanics modeling, Langmuir 31 (2015) 3934–3943. https://doi/10.1021/acs.langmuir.5b00671.
[16] P. Crespo, P. de la Presa, P. Marín, M. Multigner, J.M. Alonso, G. Rivero, F. Yndurain, J.M. González-Calbet, A. Hernando, Magnetism in nanoparticles: tuning properties with coatings, J. Phys. Condens. Matter 25 (2013) 484006.
[17] Y. Zhang, Y. Du, H. Xu, Q. Wang, Diverse-shaped iron sulfide nanostructures synthesized from a single source precursor approach, Cryst. Eng. Comm. 12 (2010) 3658–3663. https://doi/:10.1039/c002824j.
[18] I.S. Lyubutin, S.S. Starchikov, C.-R. Lin, S.-Z. Lu, M.O. Shaikh, K.O. Funtov, T. V. Dmitrieva, S.G. Ovchinnikov, I.S. Edelman, R.D. Ivantsov, Magnetic, structural, and electronic properties of iron sulfide Fe_3S_4 nanoparticles synthesized by the polyol mediated process, J. Nanoparticle Res. 15 (2013) 1397. https://doi/10.1007/s11051-012-1397-0.
[19] J.W. Thomson, K. Nagashima, P.M. Macdonald, G.A. Ozin, From sulfur −Amine solutions to metal sulfide nanocrystals: peering into the Oleylamine− sulfur black box, J. Am. Chem. Soc. 133 (2011) 5036–5041, https://doi.org/10.1021/ja1109997.
[20] Bruker, AXS TOPAS V4: General Profile and Structure Analysis Software for Powder Diffraction Data. – User's Manual, Bruker AXS, Karlsruhe, Germany, 2008.
[21] D.A. Petrov, C.R. Lin, R.D. Ivantsov, S.G. Ovchinnikov, S.M. Zharkov, G.Y. Yurkin, D.A. Velikanov, Y.V. Knyazev, M.S. Molokeev, Y.T. Tseng, E.S. Lin, I.S. Edelman, A. O. Baskakov, S.S. Starchikov, I.S. Lyubutin, Characterization of the iron oxide phases formed during the synthesis of core-shell Fe_xO_y@C anoparticles modified with Ag, Nanotechnology 31 (2020) 395703. https://doi/10.1088/13616528/ab9af2.
[22] S.H. Li, Y.-H. Chen, J.-J. Lee, H.-S. Sheu, Phase transition of iron sulphides minerals under hydrothermal conditions and magnetic investigations, Phys. Chem. Miner. 45 (2018) 27–38, https://doi.org/10.1007/s00269-017-0898-x.
[23] R. Suja, V. Sanyal, Spectral analysis of zinc and nickel doped iron sulphide nanomaterials assisted with cationic surfactant, AIP Conf. Proc. 2117 (1–9) (2019), 020008, https://doi.org/10.1063/1.5114588.
[24] T. Mishra, R.K. Sahu, S.-H. Lim, L.G. Salamanca-Riba, S. Bhattacharjee, Hexadecylamine capped silver and gold nanoparticles: comparative study on formation and self-organization, Mater. Chem. Phys. 123 (2010) 540–545. https://doi:10.1016/j.matchemphys.2010.05.011.
[25] M. Lashanizadegan, G. Farzi, N. Erfani, Synthesis and surface modification of aluminum oxide nanoparticles, J. Ceram. Process. Res. 15 (2014) 316–319.
[26] R.E. Vandenberghe, E. de Grave, P.M.A. de Bakker, M. Krs, J.J. Hus, Mössbauer effect study of natural greigite, Hyperfine Interact. 68 (1992) 319–322, https://doi.org/10.1007/BF02396500.
[27] H. Stanjek, E. Murad, Comparison of pedogenic and sedimentary greigite by X-ray diffraction and mössbauer spectroscopy, Clay Clay Miner. 42 (1994) 451–454, https://doi.org/10.1346/CCMN.1994.0420411.
[28] V. Hoffmann, H. Stanjek, E. Murad, Mineralogical, magnetic and Mössbauer data of smythite (Fe_9S11), Studia geoph, et geod. 37 (1993) 366–381, https://doi.org/10.1007/BF01613583.
[29] S. Mourdikoudis, L.M. Liz-Marzán, Oleylamine in nanoparticle synthesis, Chem. Mater. 25 (2013) 1465–1476. https://doi:10.1021/cm4000476.
[30] C.-R. Lin, Y.-T. Tseng, S.G. Ovchinnikov, R.D. Ivantsov, I.S. Edelman, A.S. Fedorov, A.A. Kuzubov, D.A. Fedorov, S.S. Starchikov, I.S. Lyubutin, Fe_3S_4 and Fe_3O_4 magnetic nanocrystals: magnetooptical and Mössbauer spectroscopy study, Mater. Res. Express 1 (2014) 025033. https://doi:10.1088/2053-1591/1/2/025033.